Charge transfer, excitation and evaporation in low energy collisions of simple metal clusters and fullerenes with atomic targets

ARTICLE *in* NUCLEAR INSTRUMENTS AND METHODS IN PHYSICS RESEARCH SECTION B BEAM INTERACTIONS WITH MATERIALS AND ATOMS · MAY 2003

Impact Factor: 1.12 · DOI: 10.1016/S0168-583X(02)01963-8

Available online at www.sciencedirect.com
SCIENCE DIRECT®
ELSEVIER
Nuclear Instruments and Methods in Physics Research B 205 (2003) 677–683
NIM B
Beam Interactions with Materials & Atoms
www.elsevier.com/locate/nimb

Charge transfer, excitation and evaporation in low energy collisions of simple metal clusters and fullerenes with atomic targets

P.-A. Hervieux [a,*], L.F. Ruiz [b], B. Zarour [c], M.F. Politis [d], J. Hanssen [a], F. Martín [b]

[a] LPMC, Institut de Physique, Technopôle 2000, 57078 Metz Cedex 03, France
[b] Departamento de Química C-9, Universidad Autónoma de Madrid, 28049 Madrid, Spain
[c] MPI für Physik Komplexer Systeme, Nöthnitzer Strasse 38, D-01187 Dresden, Germany
[d] GPS, Université Paris 7, 2 Place Jussieu 75251 Paris Cedex 05, France

Abstract

We present charge transfer, excitation and evaporation cross sections in low energy collisions of small and medium-size metal clusters (Na_n^{q+}, Li_n^{q+}) and C_{60} with atomic targets (H^+, He^{2+} and Cs) using a molecular close-coupling formalism and a post-collision rate equation model. The theoretical model benefits from different time scales associated with the collision and the internal motion of the cluster nuclei. The collision description includes the many-electron aspect of the problem and makes use of a realistic cluster potential obtained with density functional theory and a spherical jellium model. The evaporation model takes into account the non-harmonic effects of the ionic motion and describes sequential evaporation to any order within the framework of the microcanonical statistical model of Weisskopf. We show that the relative abundance of different fragments depends critically on the cluster temperature and the spectrometer time of flight window. We have found good agreement with recent experimental results [Eur. Phys. J. D 12 (2000) 185].

PACS: 36.40.Sx; 36.40.Qv; 82.30.Fi
Keywords: Cluster–atom collision; Molecular time-dependent; Fragmentation of atomic clusters

1. Introduction

Charge transfer (CT), excitation and fragmentation occur in numerous physical and chemical processes involving atomic, molecular or biological species and surfaces. The fundamental aspects of these processes have been thoroughly investigated in atomic and small molecular systems since the early days of quantum mechanics, while surfaces have recently entered the scene in connection with technological applications. The study of CT and excitation with clusters have received much less attention. In a series of papers, we have investigated CT and excitation in collisions of slow

* Corresponding author. Tel.: +33-388107182; fax: +33-388107245.
E-mail address: hervieux@sciences.univ-metz.fr (P.-A. Hervieux).

0168-583X/02/$ - see front matter © 2002 Elsevier Science B.V. All rights reserved.
doi:10.1016/S0168-583X(02)01963-8

protons with neutral [2–4] and positively charged [5,6] closed-shell Na clusters using a many-electron quantum dynamical theory. These theoretical predictions have not yet been confirmed experimentally. This is due to the fact that production of mass-selected neutral cluster beams is much less effective than that of charged clusters, which makes neutral clusters difficult to use in collision experiments. For this reason, in recent works, we have extended the former studies to collisions of charged clusters with neutral atoms [7,8]. Good agreement with experiment has been found, which validates the conclusions found in our earlier works. On the light of these new results, we present, in a unified way, the general trends that govern CT and excitation in these processes, paying a special attention to the cluster break up after the collision. To analyse the latter aspect, we have evaluated partial cross sections corresponding to the different fragmentation channels in $Li_{31}^{2+} + Cs$ collisions; these results are compared with very recent experimental results [9]. We also present the results of improved calculations for single and double CT in $He^{2+} + C_{60}$ collisions, which show that double CT is even larger than predicted in previous work [10]. Atomic units are used throughout unless otherwise stated.

2. Theoretical methods

2.1. General considerations

Our method benefits from the different time scales associated with the collision and the internal motion of the cluster nuclei. In the first place, because the collision time ($\tau_{col} = 10^{-14}$ s) is much shorter than the cluster vibration period ($\tau_v = 10^{-12}$ s) in the range of impact velocities considered in this work ($v \approx 0.01$–0.04). In the second place, because clusters that are electronically excited during the collision relax their excess energy once the collision is over (the electron–phonon coupling responsible for the observed dissociation has a characteristic lifetime $\tau_{rel} = 10^{-13}$–10^{-12} s and, therefore, can be ignored during the collision). As a consequence, the only nuclear degree of freedom (DOF) that is relevant in the collision dynamics is the relative distance R between the cluster and the atomic species. Furthermore, evaporation is a post-collisional effect that can be described separately provided that the collisional energy deposit δE and the initial cluster temperature is known. Still, dissociation may be induced in frontal collisions with the target, but this will not be taken into account because the experimental results show that, in general, it is a minor dissociation channel at low impact velocities (a similar situation can be found in [11,12]). According to the above discussion, the collision and the subsequent evaporation process have been treated separately, being δE the connection between these two problems.

2.2. Electron dynamics

A fully microscopic description including all the active electrons of the problem as well as all the nuclear DOFs is only possible for small metal clusters (typically containing less than 10 atoms [13,14]). The work of [2,3] have shown that, for medium-size closed-shell metal clusters, it is still possible to account for the many-electron aspect of the problem by freezing the cluster nuclear DOFs during the collision (see discussion above). The simplest way to implement such an idea is using the spherical jellium model (SJM) [15], which consists in replacing the real ionic core potential by a constant positive background of radius $R_C = r_s N^{1/3}$ where r_s is the Wigner–Seitz radius of the metal. As discussed in [8,16], this model is appropriate to describe the electronic structure of metal clusters. In the same spirit, an extension of the SJM of Puska and Nieminen [17] has been used to describe the electronic structure of C_{60} [10]. In this context, we apply the Kohn–Sham formulation of density functional theory and describe the cluster electron density in terms of single-particle orbitals. The corresponding one-electron potentials, V_C, are obtained using a local-density approximation with exchange, correlation and a self-interaction correction (see [2] for details). The latter correction ensures the correct asymptotic behaviour of the potential, $-(1+q)/r$, where q is the cluster charge. This is crucial in the present study because capture and excitation processes

occur mainly at large distances. The dynamical treatment has been described in detail in [2]. It is inspired by the molecular approach of ion–atom collisions and, therefore, it is aimed to investigate collisions at impact velocities smaller than that of cluster electrons. The consequence of the quasi-separability of the cluster Hamiltonian is that the N-electron Hamiltonian $\hat{H}$ of the cluster-proton or cluster-atom compound can be written as a sum of one-electron effective Hamiltonians,

$$\hat{H} = \sum_{i=1}^{N} \hat{h}(i). \tag{1}$$

The $\hat{h}$ Hamiltonian is given by

$$\hat{h} = -\frac{1}{2}\nabla^2 + V_{\mathrm{A}}(|\vec{r} - \vec{R}|) + V_{\mathrm{C}}[\rho(\vec{r})], \tag{2}$$

where V_{A} is the atomic target potential (Coulomb potential for H^+, He^{2+} and a model potential for the Cs atom [7]) and V_{C} is the cluster potential which is a functional of the electronic density [2]. Thus, the N-body dynamical treatment reduces to the study of N single-particle problems, which is equivalent to the independent electron model (IEM) of atomic collisions. We treat the collision in the framework of the impact parameter method, i.e. the projectile follows a straight line trajectory whereas the electrons are described quantum mechanically. Assuming that each electron i is initially in a $\phi_i(\vec{r})$ spin orbital of energy ε_i, then one has to solve a set of N time-dependent Schrödinger equations

$$\hat{h}\psi_i(\vec{r}, t) = i\frac{\mathrm{d}}{\mathrm{d}t}\psi_i(\vec{r}, t) \quad i = 1, \ldots, N, \tag{3}$$

where each $\psi_i(\vec{r}, t)$ is subject to the initial condition

$$\lim_{t \to -\infty} \psi_i(\vec{r}, t) = \phi_i(\vec{r}) \exp[-i\varepsilon_i t]. \tag{4}$$

The transition probability to a specific final configuration $(f_1, \ldots, f_N) = \|\phi_{f_1}, \ldots, \phi_{f_N}\|$ is given by the $(N \times N)$ determinant [18]

$$P_{f_1,\ldots,f_N} = \det(\gamma_{nn'}); \quad n, n' = 1, \ldots, N, \tag{5}$$

where $\gamma_{nn'}$ is the one-particle density matrix, $\gamma_{nn'} = \langle f_n|\hat{\rho}|f_{n'}\rangle$ and $\hat{\rho}$ is the density operator which accounts for the time evolution of the spin orbitals,

$$\hat{\rho}(\vec{r}, \vec{r}') = \sum_{i=1}^{N} |\psi_i(\vec{r}, t = +\infty)\rangle\langle\psi_i(\vec{r}', t = +\infty)|.$$

Since all processes leading to the same final state of the projectile contribute to the measured cross section, one has to evaluate *inclusive* cross sections [18]. The inclusive probability $P_{f_1,\ldots,f_q}$ of finding q of the N electrons in the subconfiguration $(f_1, \ldots, f_q)$ while the remaining $N - q$ ones occupy any other states is given by an ordered sum over all exclusive probabilities which include that subconfiguration. This probability is given by the $(q \times q)$ determinant [18]:

$$P_{f_1,\ldots,f_q} = \det(\gamma_{nn'}); \quad n, n' = 1, \ldots, q; \ \ q < N. \tag{6}$$

The inclusive probability of finding q occupancies and $L - q$ holes, $P_{f_1,\ldots,f_q}^{f_{q+1},\ldots,f_L}$, can be written in terms of probabilities (6) related only to occupancies (see [18]). To solve the time-dependent Schrödinger equations associated with the single-particle Hamiltonian of Eq. (1), we have expanded the one-electron wave functions in a basis of Born–Oppenheimer (BO) *molecular* states $\{\chi_k(\vec{r}, R)\}$. These states have been obtained by diagonalizing $\hat{h}$ in a two-center *atomic* basis built from spherical gaussian-type orbitals (GTO). The origin of electronic coordinates has been placed on the heaviest center (i.e. the cluster center) and the GTO's are centred around each center (projectile and target). For each collisional system, the choice of the basis states (i.e. type and number of GTO's included in the calculation) has been done very carefully in order to fully describe capture and excitation processes in the energy domain investigated.

2.3. Fragmentation dynamics

δE can be easily evaluated from the calculated transition amplitudes to cluster excited states. To obtain the total internal energy of the cluster one has to add its initial thermal energy. For a given temperature, the latter has been obtained from the experimental curve relating temperature and internal energy of bulk sodium [19]. The total internal energy is then used to evaluate the evaporation rate constants in the framework of the microscopic and microcanonical statistical theory

of Weisskopf [20]. Dissociation energies of the different fragments have been taken from experiment [21]. Anharmonic effects are included by employing the level density obtained from the specific entropy of bulk sodium [19]. The calculated rate constants are used to build a system of differential equations that includes both monomer and dimer evaporation as well as sequential evaporation events up to any order. Time integration is performed up to the value of the experimental time of flight (TOF). This leads to branching ratios for the different fragments and, hence, to partial cross sections.

3. Collisions with atomic ions

3.1. Cluster size dependence of CT and excitation cross sections

We first consider the collision $H^+ + Na_n$ for different values of n. The neutralization and excitation cross sections are shown in Fig. 1 as functions of impact energy. In all cases, the total excitation cross sections are smaller than the neutralization cross sections. We can observe that the latter increase with impact energy for the smaller systems, Na_8 and Na_{20}, and are practically flat for the larger ones, Na_{40} and Na_{92}. In contrast, excitation cross sections are increasing functions of impact energy in all cases. It can be also observed that both capture and excitation cross sections increase with cluster size; in contrast the rate of this increase decreases with size. This is more clearly shown in Fig. 2, where we have plotted the calculated capture cross section as functions of cluster size for impact energies of 62.5 and 360 eV. In the latter figure we have included for comparison the value of the corresponding geometrical cross sections, $\sigma_{geom} = \pi R_C^2$. We conclude from this comparison that (i) the neutralization cross section is much larger than the geometrical cross section and (ii) the rate of increase is not due to purely geometrical effects. The observed behaviour is related to the position of the avoided crossings

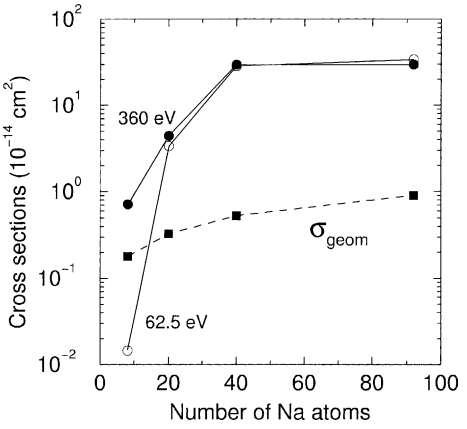

Fig. 2. Capture cross sections as functions of the number of cluster sodium atoms for two different values of the impact energy. The dashed line is the geometrical cross section obtained with the formula $\sigma_{geom} = \pi R_C^2$.

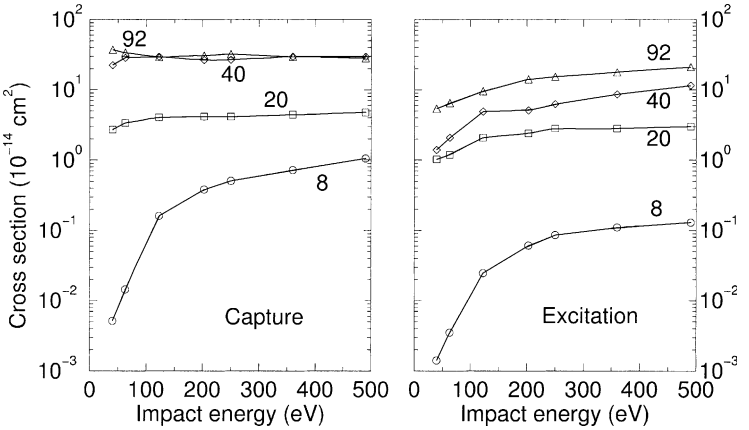

Fig. 1. Electron capture and excitation cross sections for $H^+ + Na_n$ collisions. Numbers indicate values of n.

between capture channels and the states dissociating into occupied orbitals of the cluster (see [4]).

3.2. Cluster charge dependence of CT and excitation cross sections

We consider now the collision of isoelectronic Na_{20+q}^{q+} clusters with H^+. The neutralization and excitation cross sections are shown in Fig. 3 as functions of impact velocity in the range $v = 0.02$–0.14 a.u. (40–500 eV). For $Na_{19}^- + H^+$ and $Na_{20} + H^+$ collisions, the neutralization cross sections are larger than the geometrical cross section (which is of the order of 100 Å) and larger than the total excitation cross sections. They are comparable for the $Na_{20}^+ + H^+$ collision (see [6] for details concerning post-collisional fragmentation effects in this particular case). The neutralization cross section significantly decreases with cluster charge. This is what one would expect at first sight since the interaction potential between the proton and the target is attractive for $Na_{19}^- + H^+$, less attractive (polarization-like) for $Na_{20} + H^+$ and repulsive $Na_{21}^+ + H^+$. One would also expect a smaller neutralization cross section for $Na_{22}^{2+} + H^+$ because the potential is even more repulsive. The difference between neutralization cross sections are smaller at the higher impact velocities because couplings at small internuclear distances become more efficient (as observed in ion–atom collision at low energies).

3.3. Single and double electron capture in collisions of He^{2+} with C_{60}

The single and double CT cross sections are given in Fig. 4 as functions of impact energy. For all impact velocities, single CT cross sections are comparable to double CT cross sections. The former slightly increases with impact energy, while the latter decreases. In [10] we have investigated charge exchange in collisions of protons and α particles with C_{60} in the same impact velocity range 0.04–0.14 a.u. (which corresponds to reduced energies of 40–500 eV/amu). In that work we found that, for H^+ projectiles, CT occurs near the cluster surface and, therefore, the corresponding cross section should be comparable to the geometrical cross section of C_{60}. In contrast, for He^{2+} projectiles, CT occurs far outside the cluster and, therefore, the calculated CT cross sections are significantly larger than the geometrical cross

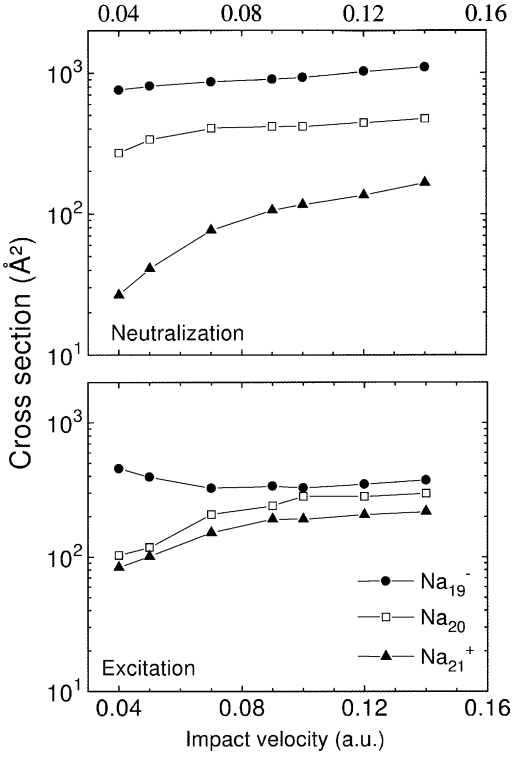

Fig. 3. Neutralization and excitation cross sections for $H^+ + Na_{20+q}^{q+}$ collisions.

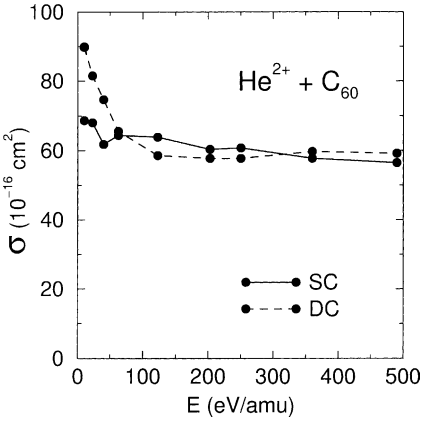

Fig. 4. Single (SC) and double (DC) charge-exchange cross sections for $He^{2+} + C_{60}$ collisions.

sections. In particular, the double CT cross section shown in Fig. 4 is significantly larger than that reported in [10]. This is due to the inclusion of more capture channels in the corresponding inclusive probabilities. The value of the double CT is extremely large compared with that observed in ion–atom collisions. It must be pointed out that we have not included correlation effects in our description of the doubly excited states of the neutralized He atom. However, this is a reasonable approximation for total double CT cross sections because the latter must be obtained by adding contributions from several doubly excited states and this is almost equivalent to sum over IEM configurations.

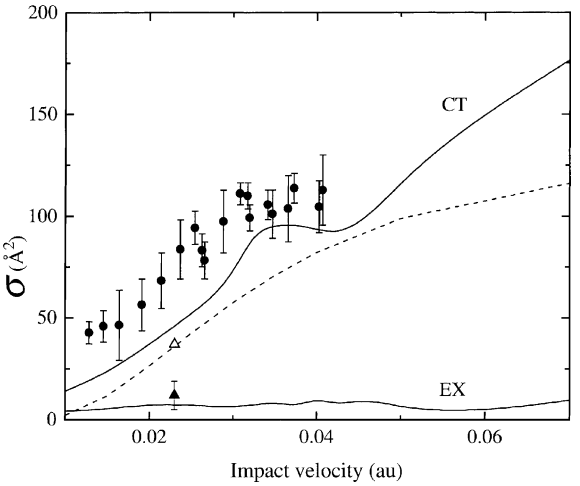

Fig. 5. Integral charge transfer (CT) and excitation (EX) cross sections for $Na_9^+ + Cs$ collisions as functions of impact velocity. Full lines: present results; dashed line: Landau–Zener model for CT [7]; open triangles: theoretical result of Knospe et al. at $T = 0$ K [11] for CT; full circles: experimental results of Bréchignac et al. [1] for CT; full triangles: experimental result of Bréchignac et al. for CT [22].

4. Collisions with neutral atomic targets

In this case, the projectile must be a positively charged cluster. A detailed theoretical study of evaporation and fragmentation in $Na_9^+ + Cs$ collisions for impact velocities $v > 0.01$ a.u. has been given in [7,8]. The various fragments that are observed experimentally are due to two different processes: (i) charge transfer induced evaporation (CTE) and (ii) collision induced dissociation (CID). CTE is roughly two orders of magnitude larger than CID, so that most fragments arise from neutral Na_9 clusters, which mainly evaporate monomers and dimers. Our results for the integral CT cross sections are in good agreement with the experimental results, as illustrated in Fig. 5 [7]. In this case, comparison with experimental CTE and CID cross section is not straightforward due to the absence of absolute measurements. For this reason, we present here the results of a similar study for the collision of Li_{31}^{2+} ions with Cs atoms. The main advantage of choosing such a system is that, while CT leads to neutral species when singly charged cluster projectiles are used, CT products in the present case are also charged and, therefore, evaporative fragments can be easily detected and identified by mass spectrometry. In order to study this process, we have used the sequential evaporation model described in Section 2.3. The rate constant are obtained from the calculated collisional energy deposits. We show in Fig. 6 that CTE cross sections critically depend on the cluster temperature T and the TOF window τ_e. Using the experimental values $T = 450$ K and $\tau_e = 3$ μs [9], we obtain a very good agreement with experiment. In particular, the theoretical results confirm that, at $T = 450$ K, the dominant fragment is Li_{30}^+, followed by Li_{31}^+ and Li_{29}^+ in almost similar proportions. It can be clearly seen that Li_{30}^+ is only dominant in the range $\tau_e = 10^{-6}$–10^{-5} s. For shorter TOF, Li_{31}^+ clusters produced by CT have not enough time to dissociate and, consequently, little evaporation is observed. The opposite occurs for $\tau_e > 10^{-5}$ s. Similar strong variations are observed for other values of T. A comparison of the results at 300, 390 and 450 K for a fixed value of $\tau_e = 3$ μs shows that evaporation is strongly modified by temperature: while Li_{31}^+ is the dominant species at $T = 390$ K, it has practically disappeared at 450 K. Thus, good agreement between theory and experiment is only possible by using the experimental value of the TOF and a cluster temperature consistent with the experimental distribution. Small deviations from this choice lead to enormous differences in partial cross sections and, therefore, to very different physical interpretations.

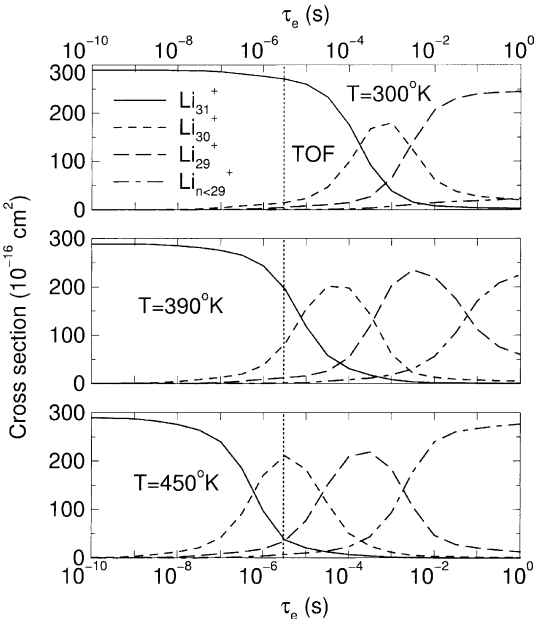

Fig. 6. Calculated CTE cross sections for $Li_{31}^{2+} + Cs$ collisions as functions of TOF for three values of temperature. The vertical dashed line represents the TOF of the present experiment [9].

Similarly, any deficiency in the theoretical treatment may lead to results in complete disagreement with experiment.

References

[1] C. Bréchignac, Ph. Cahuzac, B. Concina, J. Leygnier, I. Tignères, Eur. Phys. J. D 12 (2000) 185.
[2] M.F. Politis, P.-A. Hervieux, J. Hanssen, M.E. Madjet, F. Martín, Phys. Rev. A 58 (1998) 367.
[3] F. Martín, P.-A. Hervieux, J. Hanssen, M.E. Madjet, M.F. Politis, Phys. Rev. B 58 (1998) 6752.
[4] F. Martín, M.F. Politis, B. Zarour, P.-A. Hervieux, J. Hanssen, M.E. Madjet, Phys. Rev. A 60 (1999) 470.
[5] B. Zarour, J. Hanssen, P.-A. Hervieux, M.F. Politis, F. Martín, Phys. Rev. A 65 (2002) 033201.
[6] M.F. Politis, P.-A. Hervieux, J. Hanssen, M.E. Madjet, F. Martín, in: J.L. Duggan, I.L. Morgan (Eds.), Applications of Accelerators in Research and Industry, CP475, American Institute of Physics, NewYork, 1999, p. 391.
[7] B. Zarour, J. Hanssen, P.-A. Hervieux, M.F. Politis, F. Martín, J. Phys. B 33 (2000) L707.
[8] P.-A. Hervieux, B. Zarour, J. Hanssen, M.F. Politis, F. Martín, J. Phys. B 34 (2001) 3331.
[9] C. Bréchignac, Ph. Cahuzac, B. Concina, J. Leygnier, L.F. Ruiz, B. Zarour, P.-A. Hervieux, J. Hanssen, M.F. Politis, F. Martín, Phys. Rev. Lett. 89 (2002) 183402.
[10] L.F. Ruiz, P.-A. Hervieux, J. Hanssen, M.F. Politis, F. Martín, Int. J. Quant. Chem. 86 (2002) 106.
[11] O. Knospe, J. Jellinek, U. Saalmann, R. Schmidt, Phys. Rev. A 61 (2000) 022715.
[12] C. Bréchignac, Ph. Cahuzac, B. Concina, J. Leygnier, Eur. Phys. J. D 16 (2001) 91.
[13] U. Saalmann, R. Schmidt, Phys. Rev. Lett. 80 (1998) 3213.
[14] O. Knospe, J. Jellinek, U. Saalmann, R. Schmidt, Eur. Phys. J. D 5 (1999) 1.
[15] W. Ekardt, Phys. Rev. B 29 (1984) 1558.
[16] M. Brack, Rev. Mod. Phys. 65 (1993) 677.
[17] M.J. Puska, R.M. Nieminen, Phys. Rev. A 47 (1993) 1181.
[18] H.J. Lüdde, R.M. Dreizler, J. Phys. B 18 (1985) 107.
[19] R. Hultgren, R.L. Orr, P.D. Anderson, K.K. Kelley, Selected Values of Thermodynamic Properties of Metals and Alloys, Wiley and Sons, New York, 1963, 326.
[20] P.-A. Hervieux, D.H.E. Gross, Z. Phys. D 33 (1995) 295.
[21] C. Bréchignac, Ph. Cahuzac, J. Leygnier, J. Weiner, J. Chem. Phys. 90 (1989) 1492.
[22] C. Bréchignac, Ph. Cahuzac, J. Leygnier, R. Pflaum, J. Weiner, Phys. Rev. Lett. 61 (1988) 314.